Advanced Composite Materials
Publication details, including instructions for authors and subscription information:
http://www.tandfonline.com/loi/tacm20

Prediction of Tensile Strength of Unidirectional CFRP Composites

T. Okabe [a], K. Ishii [b], M. Nishikawa [c] & N. Takeda [d]

[a] Department of Aerospace Engineering, Tohoku University, 6-6-01 Aoba-yama, Aoba-ku, Sendai 980-8579, Japan

[b] Airframe Section, Engineering Department, Japan Airlines International, Japan

[c] Department of Nanomechanics, Tohoku University, Japan

[d] Department of Advanced Energy, The University of Tokyo, Japan

Version of record first published: 02 Apr 2012.

To cite this article: T. Okabe , K. Ishii , M. Nishikawa & N. Takeda (2010): Prediction of Tensile Strength of Unidirectional CFRP Composites, Advanced Composite Materials, 19:3, 229-241

To link to this article: http://dx.doi.org/10.1163/092430409X12605406698273

VSP

Advanced Composite Materials 19 (2010) 229–241

ADVANCED COMPOSITE MATERIALS
brill.nl/acm

Prediction of Tensile Strength of Unidirectional CFRP Composites

T. Okabe [a,*], **K. Ishii** [b], **M. Nishikawa** [c] **and N. Takeda** [d]

[a] Department of Aerospace Engineering, Tohoku University, 6-6-01 Aoba-yama, Aoba-ku, Sendai 980-8579, Japan

[b] Airframe Section, Engineering Department, Japan Airlines International, Japan

[c] Department of Nanomechanics, Tohoku University, Japan

[d] Department of Advanced Energy, The University of Tokyo, Japan

Received 3 June 2009; accepted 23 June 2009

Abstract

The tensile strength of unidirectional carbon fiber-reinforced plastic (CFRP) composites was predicted by numerical simulation plus size scaling. The fiber strength distribution used in the numerical simulation was determined from the fragmentation process in a single fiber composite. Since the experimental data obviously did not fit the normal Weibull distribution, we fitted them with the Weibull of Weibull model, considering the statistical distribution of scale parameters of fiber strength in the normal Weibull model. Moreover, the constitutive law of the matrix was derived from the stress–strain curves of the angle ply laminates, utilizing the micromechanics approach proposed by Tohgo *et al.* [9]. Based on these parameters, we simulated the tensile fracture of unidirectional CFRP composites with the spring element model (SEM). The predicted tensile strength by numerical simulation plus size scaling agreed well with the experimental data. The results also confirmed that the Weibull of Weibull model is important to predict size-dependent composite strength.

Keywords

Fiber-reinforced composite, tensile strength, spring element model, size scaling, micromechanics

1. Introduction

Carbon fiber-reinforced plastic (CFRP) composites are a main material for aeronautical applications because of their specifically high strength and stiffness. To use this material safely in aeronautical applications, the establishment of its strength prediction is essential. The strength of unidirectional fiber composites is especially important when failure occurs in the direction normal to the fiber axis, since it di-

* To whom correspondence should be addressed. E-mail: okabe@plum.mech.tohoku.ac.jp
Edited by the JSCM

DOI:10.1163/092430409X12605406698273

rectly affects the strength of the entire composite structure. Therefore, many studies predicting the strength of unidirectional fiber-reinforced composites have been reported in the literature [1–7]. These studies have pointed out that both estimating the fiber strength statistics and the constitutive law of the matrix and using the full 3D numerical model are important in predicting composite tensile strength.

In this study, we experimentally measured fiber strength distribution through single fiber composite tests and the constitutive law of the epoxy matrix, using the stress–strain curve of unidirectional angle ply laminates, and then predicted the tensile strength of unidirectional CFRP composites (T300/F593).

This paper is organized as follows. First, we estimated the parameters of fiber strength distribution by fitting the fragmentation theory [8] with the experimental results of a single fiber composite. The single fiber composite is a useful tool to evaluate fiber strength distribution along the fiber, since the fragmentation process can be observed in it. However, the fragmentation processes vary among samples. Thus, we used the Weibull of Weibull model [5] to account for these variations. Second, we obtained the constitutive law of the matrix using the stress–strain curve of the unidirectional angle ply laminates. The stress–strain curve of the unidirectional angle ply laminates is nonlinear due to the plasticity of the matrix. In this study, the constitutive law of the matrix is estimated from the nonlinear stress–strain curve of the unidirectional angle ply laminates using the incremental Mori–Tanaka approach [9]. Third, based on these data, we predicted the tensile strength of the unidirectional CFRP composites using the spring element model (SEM) [10, 11], which was preliminarily evaluated by comparison with 3D finite element analysis. The predicted results agreed well with the experimental data. The results confirmed that the tensile strength of the unidirectional CFRP composites could be predicted by both direct estimation of properties including the fiber strength and constitutive relation, and the numerical model.

2. Estimation of Fiber Strength Distribution Using a Single Fiber Composite

In this experiment, T300™ carbon fiber (Toray Co. Ltd.) was used to fabricate a single fiber composite. Bisphenol-A Epoxy resin (Epikote 828) and curing agent triethylenetetramine (EpikureTETA) were used to form a matrix in 100/11 ratios. All samples were initially cured at 50°C for 80 min, and then post-cured at 100°C for 60 min. A loading machine built under an optical microscope was used for the fragmentation test. The fiber breaks in a single fiber composite were counted with the optical microscope. In this study, 0.05% strain per minute was applied to the specimen. The fragmentation tests were conducted 20 times to investigate the variation between samples.

Figure 1 indicates the number of fiber breaks in a single fiber composite *versus* applied fiber stress. To consider the residual compressive strain in a fiber, the applied fiber stress was calculated by multiplying the Young's modulus by the strain in which the residual compressive strain is subtracted from the applied strain. The

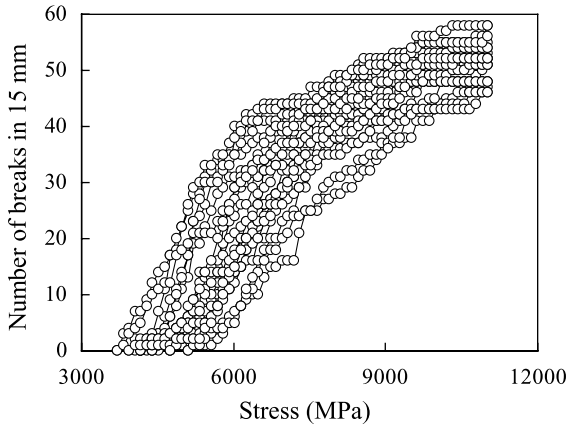

Figure 1. Number of breaks *versus* applied fiber stress for twenty specimens of single fiber composite.

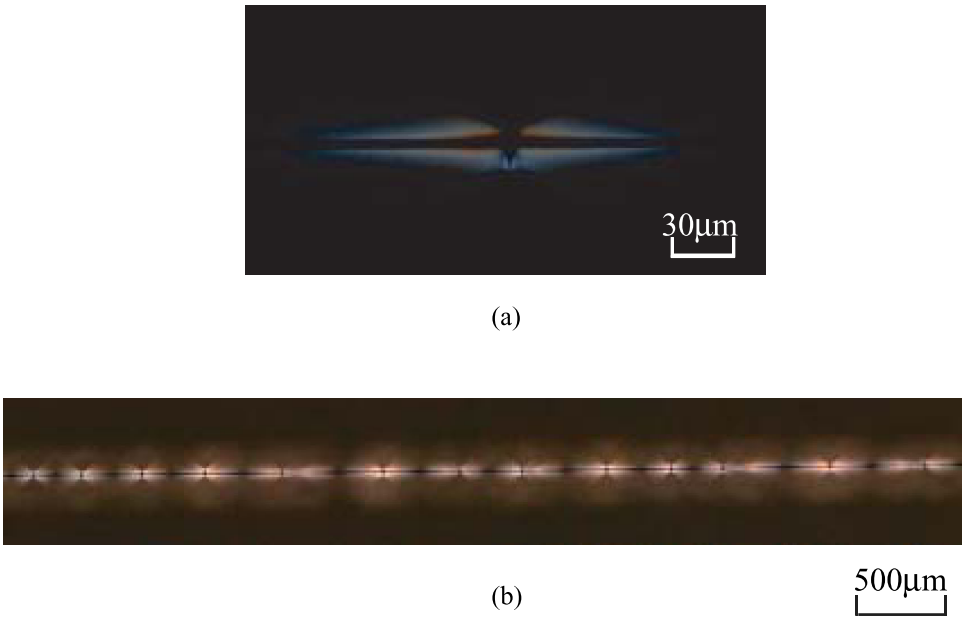

Figure 2. Birefringence pattern (a) around a fiber break and (b) along the fiber. This figure is published in color online, see http://www.brill.nl/acm

number of fiber breaks in a single fiber composite was not saturated even if the applied fiber stress was quite high. We have already reported that this result is due to the matrix hardening effect [12]. Figure 2 depicts the birefringence pattern in a single fiber composite. No debonding around a fiber break was observed in this single fiber composite. Moreover, the stresses of the fiber breaks are very scattered among the specimens, although the increase rates of fiber breaks are similar. This result implies that the strength is scattered among these fibers. Therefore, the conventional Weibull model cannot be applied to determine the fiber strength distribution. In this

study, we used the Weibull of Weibull model [5], which considers the distribution of characteristic strength among the fibers. Here, we briefly introduce the concept of the Weibull of Weibull model and then explain how to derive the parameters in this model from the experiments.

The Weibull of Weibull model assumes that the strength distribution of an arbitrary ith fiber with length L obeys the conventional Weibull model given by

$$P_{\mathrm{f}}^{i} = 1 - \exp\left\{\left(-\frac{L}{L_0}\right)\left(\frac{\sigma}{\sigma_0^i}\right)^{\rho'}\right\}. \tag{1}$$

It also assumes that the scale parameter σ_0^i obeys the Weibull model given by

$$F(\sigma_0^i) = 1 - \exp\left\{-\left(\frac{\sigma_0^i}{\bar{\sigma}_0}\right)^{m}\right\}. \tag{2}$$

This is the main concept of the Weibull of Weibull model.

In this study, we estimated parameters $\bar{\sigma}_0$, ρ' and m from the experimental data of fragmentation as follows:

(1) Estimate σ_0^i and ρ' for each fiber, using the Hui model [8] predicting the relationship between fiber breaks and applied fiber stress. Here, it is assumed that ρ' has a unique value for all fibers.

(2) Estimate the characteristic strength $\bar{\sigma}_0$ and Weibull parameter m of a set of fibers using the obtained strength of an arbitrary ith fiber.

The Hui model utilizes constant stress recovery model, which assumes that the matrix around the fiber is an elastic–perfect plastic material. Therefore, this model cannot explain the fragmentation process at a higher strain level. However, this model is sufficient if only the fiber strength is needed, because the fragmentation process at a lower strain level is used. This was discussed by the present authors [12].

In this study, we determined ρ' as 15, estimated the fiber strength of an arbitrary fiber, and derived the characteristic strength and Weibull parameters of a set of fibers. Table 1 presents the parameters obtained from these estimations. We used several values of interfacial yielding stress τ; however, the obtained strengths were similar to one another. This is because interfacial stress does not greatly affect the fragmentation process at a lower strain level, as shown in Fig. 3.

3. Estimation of the Constitution Law of Epoxy Matrix

The tensile strength of unidirectional composites depends on the constitutive law of epoxy (F593) matrix. In general, the constitutive law of matrix in composites is not open. In fact, the catalog of T300/F593 does not provide the stress–strain relation of the matrix. In addition, the constitutive law of matrix will be changed during

Table 1.
Statistical parameters of fiber strength

Weibull scale parameter, $\bar{\sigma}_0$ (MPa)	4443
Gage length, L_0 (mm)	50
Weibull shape parameter in P_f^i, ρ'	15
Weibull shape parameter in $F(\sigma_0^i)$, m	10.3

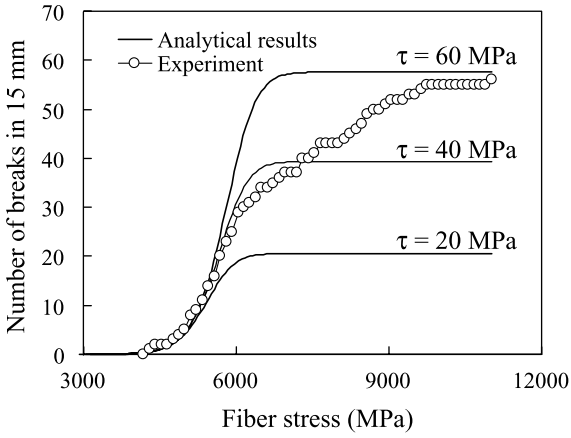

Figure 3. Predicted number of breaks *versus* applied fiber stress in comparison with experimental data from Fig. 1.

material processing. Therefore, we conducted the tensile test of unidirectional angle ply laminates to estimate the constitutive law of an epoxy matrix.

Tensile test specimens with dimensions of 120 mm (length) × 5 mm (width) × 1 mm (height) were cut from the fabricated plates, and tapered GFRP tabs were glued at both ends of the specimen to provide a gage length of 50 mm. Tensile tests were performed at a constant cross-head speed of 0.5 mm/min at room temperature in air. A computer-assisted data acquisition system was used to obtain the stress–strain curves from a strain gage placed on the specimen and a load cell. In this experiment, the unidirectional composites were tested for several angles (0°, 30°, 45°, 60°, and 90°).

Figure 4 presents the obtained stress–strain curves with the curves predicted by the micromechanics model proposed by Tohgo *et al.* [9]. This micromechanics model is based on Eshelby's inclusion approach and gives the stress–strain curves of angle ply laminates using the constitutive law of the matrix directly. In this study, the constitutive law of the matrix is inversely estimated from the stress–strain curves of angle ply laminates. In this estimation, we assume that the relationship between an equivalent stress σ_e^m and an equivalent plastic strain ε_e^{mp} is given as

$$\sigma_e^m = \sigma_Y^m \left(1 + \frac{\varepsilon_e^{mp}}{\alpha_p}\right)^{\beta_p}. \tag{3}$$

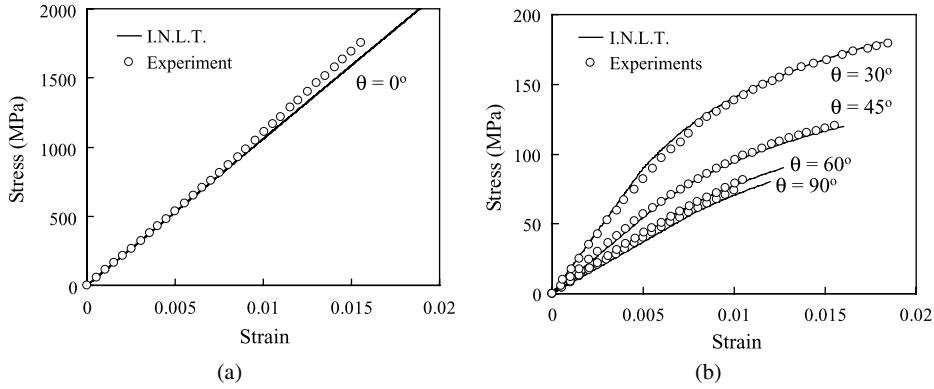

Figure 4. Stress–strain curve of unidirectional angle-ply composite: I.N.L.T. denotes the micromechanics theory proposed by Tohgo *et al.* [9]. (a) $\theta = 0°$, (b) $\theta = 30°, 45°, 60°, 90°$.

Table 2.
Material properties of carbon fiber and matrix

Fiber Young's modulus, E (GPa)	232
Fiber radius, R (μm)	3.5
Matrix shear modulus, G (GPa)	1.09
Matrix Poisson's ratio, ν_m	0.35
Matrix yield stress, σ_Y^m (MPa)	46
Matrix plasticity parameter, α_p	0.0008
Matrix plasticity parameter, β_p	0.2
Fiber volume fraction, V_f (Averaged value of the experiments)	0.53

Here, σ_Y^m, α_p, and β_p are estimated by fitting the predicted curves with experimental curves. Table 2 presents the estimation results. All strain–stress curves can be predicted by adjusting σ_Y^m, α_p, and β_p to explain the strain–stress curve of an angle ($\theta = 45°$) ply laminate.

Figure 5 depicts the estimated stress–strain curve with that of the different epoxy (#3631) reported by Ishibashi [13]. The prediction agrees well with the results for epoxy #3631. Therefore, this method is appropriate to estimate the stress–strain curve of the matrix.

4. Strength Prediction for the Unidirectional Carbon Fiber-Reinforced Composites

4.1. Tensile Tests

We conducted tensile tests for CFRP (T300/F593). Tensile test specimens with dimensions of 120 mm × 5 mm × 1 mm were cut from the fabricated plates, and tapered GFRP tabs were glued at both ends of the specimen to provide a gage

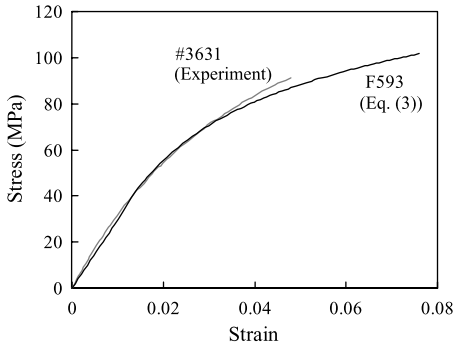

Figure 5. Predicted stress–strain curve of matrix in comparison with that of the different epoxy resin reported by Ishibashi [13].

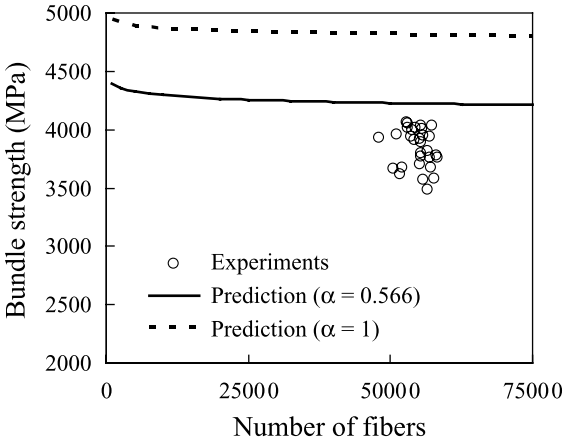

Figure 6. Predicted tensile strength *versus* number of fibers.

length of 50 mm. Tensile tests were performed at a constant cross-head speed of 0.5 mm/min at room temperature in air. A computer-assisted data acquisition system was used to obtain the stress–strain curves from a strain gage placed on the specimen and a load cell.

Figure 6 illustrates the relationship between bundle strength σ_b and the number of fibers. Bundle strength is given by

$$\sigma_b = \frac{\sigma_{UTS}^e}{V_f}, \tag{4}$$

where σ_{UTS}^e is experimental data of the tensile strength of the corresponding composite and V_f is its volume fraction. V_f was estimated from the elastic modulus of specimens, based on the mixed law.

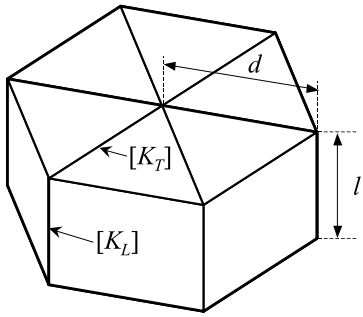

Figure 7. Schematic figure of spring element model.

4.2. Numerical Simulation

In this study, a Monte Carlo simulation is conducted using the spring element model (SEM) depicted in Fig. 7. We briefly describe the procedure of the SEM [10, 11].

The SEM consists of longitudinal and transverse elements in a 3D hexagonal arrangement (Fig. 7). The longitudinal spring element is defined as fiber; the transverse shear element is defined as matrix. The stiffness of the longitudinal and transverse elements $[K^e_{\mathrm{L}}]$, $[K^e_{\mathrm{T}}]$ are then given by

$$\left[K^e_{\mathrm{L}}\right] = \pi R^2 \int_0^l \left[B^e_{\mathrm{L}}\right]^{\mathrm{T}} E \left[B^e_{\mathrm{L}}\right] \mathrm{d}z, \tag{5}$$

$$\left[K^e_{\mathrm{T}}\right] = \frac{\pi R l}{3} \int_0^d \left[B^e_{\mathrm{T}}\right]^{\mathrm{T}} G \left[B^e_{\mathrm{T}}\right] \mathrm{d}z, \tag{6}$$

$$\left[B^e_{\mathrm{L}}\right] = \left[\frac{1}{l} \quad -\frac{1}{l}\right], \tag{7}$$

$$\left[B^e_{\mathrm{T}}\right] = \left[\frac{1}{d} \quad -\frac{1}{d}\right], \tag{8}$$

where subscripts L and T denote longitudinal and transverse elements, E is the Young's modulus, G is the effective shear modulus of the matrix, R is the fiber radius, l is the length of longitudinal elements, and d is the length of transverse elements. The SEM approximates the stress distribution within the ineffective length of a broken fiber, using the constant shear-lag model described below. Assuming that the interface shear stress τ_{s} by the matrix within the plastic region is constant, the fiber stress σ_{s} within the length of a plastic region c from a fiber break is then given by

$$\sigma_{\mathrm{s}} = \frac{2\tau_{\mathrm{s}}\bar{z}}{R}, \quad -c \leqslant \bar{z} \leqslant c, \tag{9}$$

where $\bar{z}$ is the distance from a fiber breaking point. To save calculation time, the length of plastic region c and the constant shear stress τ_{s} are given as input variables

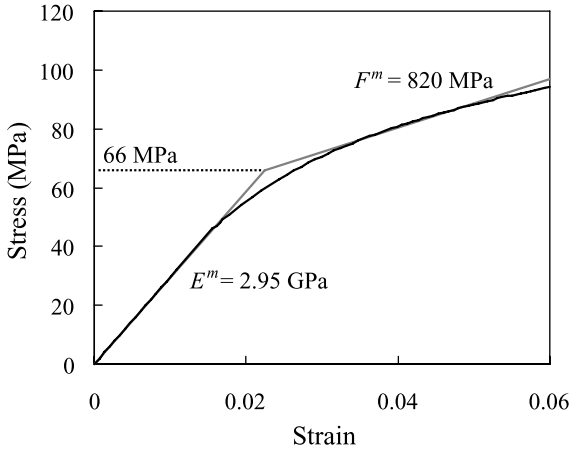

Figure 8. Stress–strain curve of matrix used in the spring element model.

with the elastic–plastic shear-lag model proposed by the present authors [12]. The equilibrium equation for the total spring-element system is then expressed as

$$\left[\sum_{e=1}^{N_{\mathrm{L}}-N_{\mathrm{B}}-N_{\mathrm{p}}}\left[K_{\mathrm{L}}^{e}\right]+\sum_{e=1}^{N_{\mathrm{T}}}\left[K_{\mathrm{T}}^{e}\right]\right]\{u\}+\sum_{e=1}^{N_{\mathrm{p}}}\pi R^{2}\int_{0}^{l}\left[B_{\mathrm{L}}^{e}\right]^{\mathrm{T}}\sigma_{\mathrm{s}}\,\mathrm{d}z=\{f\},\qquad(10)$$

where $\{u\}$ and $\{f\}$ are the vectors of nodal displacement and nodal load, respectively. N_{L} and N_{T} denote the numbers of longitudinal and transverse elements, N_{B} denotes the number of broken fiber elements, and N_{p} denotes the number of fiber elements within the length of plastic region c from fiber breaks. Equation (10) is the basic equation of the SEM. In general, the elastic–plastic problem is nonlinear and should be solved iteratively or incrementally. However, in this model, the basic equation is converted into a linear problem by assuming equation (9). In addition, the slip stress within the plastic region is estimated with the elastic–plastic shear-lag model proposed by the present authors. In this estimation, the constitutive law of the matrix obtained in the previous section is assumed as the bi-linear strain-hardening model depicted in Fig. 8.

To confirm the stress analysis of the SEM, we compared them with the 3D finite element model (FEM). Figure 9 compares stress distribution around a fiber break in the 3D FEM with that in the SEM. The 3D FEM presented in Fig. 10 is composed of 12 fibers and the matrix, represented by a 30° wedge. The 3D finite element analysis is based on the elastic–plastic (J_2 flow) constitutive law. Figure 9(a) denotes the stress distribution in the broken fiber along the fiber axis, which is normalized by the stress of intact fibers. Figure 9(b) denotes the stress concentration factor around the fiber breaking point, which is also normalized by the stress of intact fibers. The stress distributions obtained from the SEM agreed well with those of the 3D FEM.

We conducted the Monte Carlo simulation [6] for the tensile failure of the unidirectional composites using the SEM. The Weibull of Weibull model was used to

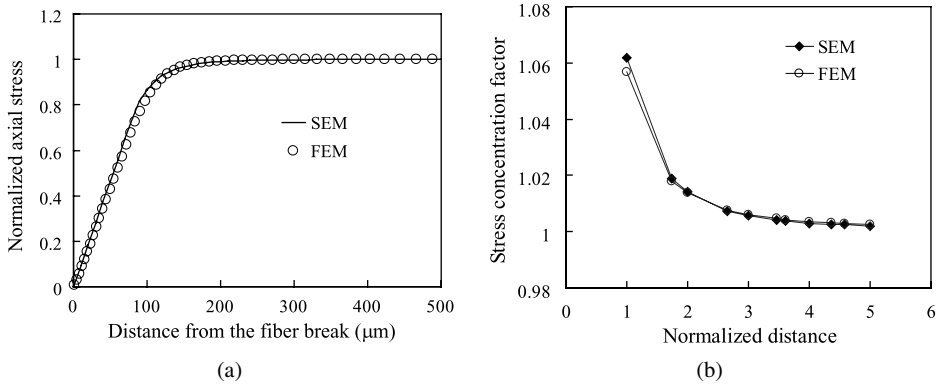

Figure 9. Comparisons of stress distribution around a fiber break: SEM and FEM denote the spring element model and the finite element model, respectively. (a) Axial stress distribution of a broken fiber; (b) axial stress concentration on nearby fibers around a broken fiber.

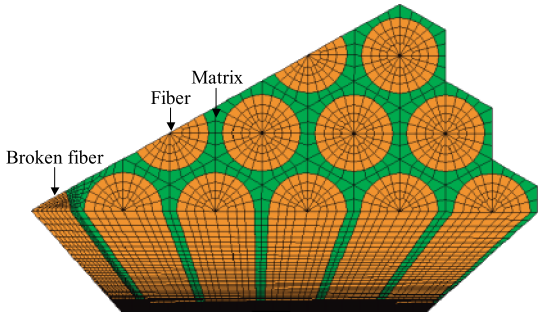

Figure 10. Finite element model having twelve fibers in unidirectional composite. The model is represented by a 30° wedge. This figure is published in color online, see http://www.brill.nl/acm

assign the strength of fiber elements. The parameters for the Weibull of Weibull are listed in Table 1. The procedure to assign the strength of fiber elements based on the Weibull of Weibull model is as follows. First the characteristic strength σ_0^i of the arbitrary ith fiber is assigned by equation (2). Then the element strengths in the ith fiber are assigned by equation (1).

The simulated model is composed of 1024 fibers and is conducted under the displacement control. The length of the model is 1 mm. In this simulation, the final failure is assumed to be in progress once the applied composite stress decreases to 90% of the applied maximum composites stress.

4.3. Simulated Results and Size Scaling

Figure 11 presents the simulated results for the stress distribution at the plane where the worst damage grows when the applied composite stress attains a peak. A cluster of the fiber breaks can be observed in this plane. Moreover, we confirmed that the cluster grew into this plane and caused a drop in applied composite stress. The

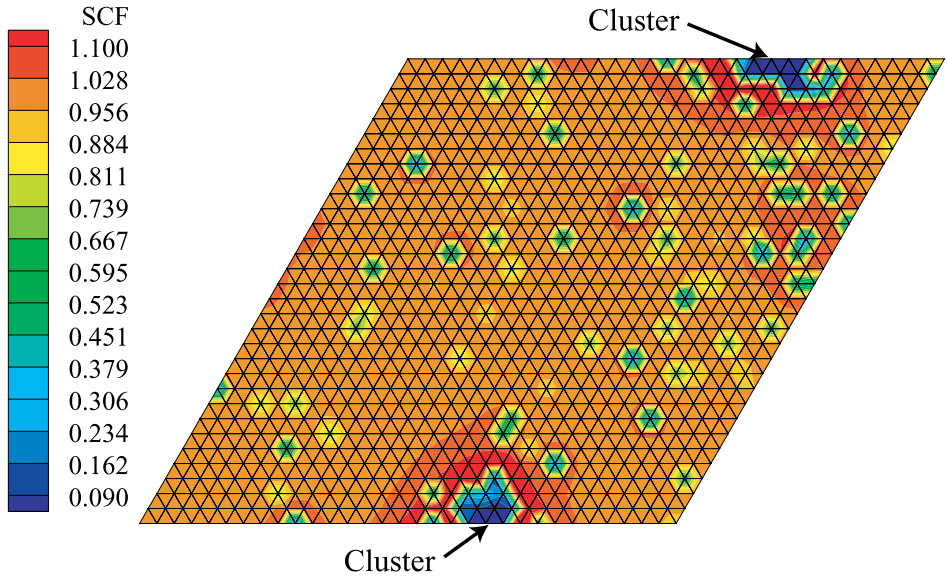

Figure 11. Distribution of the axial stress concentration factors at the final failure plane. This figure is published in color online, see http://www.brill.nl/acm

cluster is the weakest part of the composites, and the size-dependent composite strength can be explained by the weakest-link scaling when the cluster is observed in the simulation [14]. Therefore, to relate the model size with the real composite size, we conducted weakest-link scaling as follows.

This scaling assumes that the distribution of the composite strength can be explained by the phenomenological weakest-link scaling [5, 15] given by

$$P(\sigma_{\mathrm{b}}) = 1 - \exp\left[-\left(\frac{n}{n_{\mathrm{s}}}\right)\left(\frac{L}{L_{\mathrm{s}}}\right)^{\alpha}\left(\frac{\sigma_{\mathrm{b}}}{\sigma_0^{\mathrm{s}}}\right)^{m_{\mathrm{s}}}\right], \tag{11}$$

where n_{s} and L_{s} denote the number and length of fibers used in the simulation, and n and L denote the number and length of fibers in the composite with an arbitrary size. σ_0^{s} and m_{s} are the characteristic parameters of the strength distribution. α is the phenomenology parameter proposed by Watson and Smith [16] and becomes unity if the fiber strength can be explained by the conventional Weibull distribution. Curtin [5] proved that the phenomenology parameter α is given by

$$\alpha = \frac{m}{(m^2 + \rho'^2)^{1/2}}. \tag{12}$$

We fitted 100 simulated data with the strength distribution given in (11) and estimated those parameters $\sigma_0^{\mathrm{s}} = 4493$ MPa and $m_{\mathrm{s}} = 100.4$. After manipulating equation (11), the characteristic bundle strength of arbitrary composites is obtained as

$$\tilde{\sigma} = \sigma_0^{\mathrm{s}}\left(\frac{n}{n_{\mathrm{s}}}\right)^{\frac{1}{m_{\mathrm{s}}}}\left(\frac{L}{L_{\mathrm{s}}}\right)^{\frac{\alpha}{m_{\mathrm{s}}}}. \tag{13}$$

The characteristic bundle strength obtained from equation (13) is compared with the results of the experiments. The comparison is presented in Fig. 6. The prediction, which corresponds to the line denoted by $\alpha = 0.566$ calculated with equation (12), is slightly higher than the experiment data, but very close. In contrast, if the simulation assumed conventional Weibull model for fiber strength distribution and used only equation (1) by substituting $\bar{\sigma}_0$ into σ_0^i to assign the fiber element strength, the estimated parameters for composite strength distribution were $\sigma_0^s = 5069$ MPa and $m_s = 152.3$. The prediction using equation (13) was then conducted by setting $\alpha = 1$. In this case, the composite strength is much higher than that of the experiments, as shown in Fig. 6. The Weibull of Weibull model is very important to predict size-dependent composite strength.

5. Conclusions

In this study, we experimentally measured the fiber strength distribution and the constitutive law of epoxy matrix, and then predicted the tensile strength of unidirectional CFRP composites.

(1) We estimated the parameters of fiber strength (T300) distribution by fitting the fragmentation theory with the experimental results of a single fiber composite. The stresses of the fiber breaks seen in the single fiber composite were very scattered among the specimens, although the increase rates of fiber breaks were similar. We concluded that the Weibull of Weibull model, which considers the distribution of characteristic strength among the fibers, is appropriate for determining the strength distribution of T300.

(2) We obtained the constitutive law of the matrix (F593) using the unidirectional angle ply laminates. The estimated stress–strain curve was compared with that of a different epoxy (#3631) reported by Ishibashi [13]. The estimate agreed well with that of epoxy #3631. Thus, the results validated the usefulness of this approach in estimating the stress–strain curve of the matrix in composites.

(3) We predicted the tensile strength of the unidirectional CFRP (T300/F593) composites using the spring element model. The prediction was slightly higher than the experiment data, but very close. The results also confirmed that the Weibull of Weibull model is important to predict size-dependent composite strength.

References

1. K. Goda and S. L. Phoenix, Reliability approach to the tensile-strength of unidirectional CFRP composites by Monte-Carlo simulation in a shear-lag model, *Compos. Sci. Technol.* **50**, 457–468 (1994).
2. W. A. Curtin and N. Takeda, Tensile strength of fiber-reinforced composites: I. Model and effects of local fiber geometry, *J. Compos. Mater.* **32**, 2042–2059 (1998).
3. W. A. Curtin and N. Takeda, Tensile strength of fiber-reinforced composites: II. Application to polymer matrix composites, *J. Compos. Mater.* **32**, 2060–2081 (1998).

4. A. Wada and H. Fukuda, Approximate upper and lower bounds for the strength of unidirectional composites, *Compos. Sci. Technol.* **59**, 89–95 (1999).
5. W. A. Curtin, Tensile strength of fiber-reinforced composites: III. Beyond the traditional Weibull model for fiber strengths, *J. Compos. Mater.* **34**, 1301–1332 (2000).
6. T. Okabe, N. Takeda, Y. Kamoshida, M. Shimizu and W. A. Curtin, A 3D shear-lag model considering micro-damage and statistical strength prediction of unidirectional fiber-reinforced composites, *Compos. Sci. Technol.* **61**, 1773–1787 (2001).
7. K. Goda, Y. Miwa and H. Kodama, Effect of IFSS on tensile strength of unidirectional fiber composites using 3D-FEM simulation, *Adv. Compos. Mater.* **12**, 73–89 (2003).
8. C. Y. Hui, S. L. Phoenix, M. Ibnabdeljalil and R. L. Smith, The single-filament-composite test: a new statistical theory for estimating the interfacial shear strength and Weibull parameters for fiber strength, *J. Mech. Phys. Solids* **43**, 1551–1585 (1995).
9. K. Tohgo, K. Kawahara and Y. Sugiyama, Off-axis tensile properties of CFRP laminates and nonlinear lamination theory based on micromechanics approach, *Trans. Japan Soc. Mech. Engrs* **A67**, 1493–1500 (2001) (in Japanese).
10. T. Okabe, H. Sekine, K. Ishii, M. Nishikawa and N. Takeda, Numerical method for failure simulation of unidirectional fiber-reinforced composites with spring element model, *Compos. Sci. Technol.* **65**, 921–933 (2005).
11. T. Okabe, M. Nishikawa, N. Takeda and H. Sekine, Effect of matrix hardening on tensile strength of alumina-fiber reinforced aluminum matrix composites, *Acta Materialia* **54**, 2557–2566 (2006).
12. T. Okabe and N. Takeda, Elastoplastic shear-lag analysis of single-fiber composites and strength prediction of unidirectional multi-fiber composites, *Composites A* **33**, 1327–1335 (2002).
13. S. Ishibashi, *Master Thesis*, Kyoto Institute of Technology (2000) (in Japanese).
14. M. Ibnabdeljalil and W. A. Curtin, Strength and reliability of fiber-reinforced composites: Localized load-sharing and associated size effects, *Intl. J. Solids Struct.* **34**, 2649–2668 (1997).
15. Z. Xia, W. A. Curtin and P. W. M. Peters, Multiscale modeling of failure in metal matrix composites, *Acta Materialia* **49**, 273–287 (2001).
16. A. S. Watson and R. L. Smith, An examination of statistical theories for fibrous materials in the light of experimental data, *J. Mater. Sci.* **20**, 3260–3270 (1985).